Non-Isothermal Gas-Assisted Injection Molding at Low Capillary Numbers

Undergraduate Research Thesis

Presented in Partial Fulfillment of the Requirements for Graduation with Research Distinction in the College of Engineering of The Ohio State University

By

Lena Ta

William G. Lowery Department of Chemical and Biomolecular Engineering

The Ohio State University

2017

Thesis Committee:

Dr. Kurt W. Koelling, Advisor

Dr. Isamu Kusaka

Abstract

In gas-assisted injection molding (GAIM), pressurized gas is injected into a cavity filled with molten polymer to create a mold with a hollowed core. Experimentation in non-isothermal conditions at lower capillary numbers was necessary to evaluate the accuracy of a recently developed simulation model. Fractional coverage is dependent on a multitude of parameters including the mold's temperature gradient, delay time, and capillary number used. Capillary number is the ratio of viscous forces to interfacial tension and is a strong function of gas bubble velocity and fluid viscosity. Previous experiments have been performed at capillary numbers high enough to maintain the assumption that fractional coverage will plateau at a value of 0.6. This same assumption, however, cannot be used for low capillary bubble speeds. The experiments were conducted at low capillary numbers for two Newtonian fluids, and two water baths with varying temperatures were used to create a gradient. A high-speed camera captured the polymer behavior as the temperature gradient and gas injection delay time varied for each trial, and was used to determine the fractional coverage. The simulation program calculates fractional coverage with input conditions similar to the trials, and will be compared to the experimental fractional coverage. It implements a numerical solution through a hybrid control-volume finite element/finite-difference method, a momentum balance, and heat-transfer governing equations to predict wall thickness. The simulation incorporates a correcting equation at low capillary numbers to adjust for non-uniform thickness down the tube, but must be checked for any deviations from the actual. Experimental results were crucial to determine if the simulation program can accurately

make predications of more realistic process parameters. This research can become a foundation for future characterization of even more complex GAIM processes, such as ones of non-Newtonian fluids in non-isothermal, non-steady state systems.

Acknowledgments

I have immense gratitude for the advice and help that my advisor, Dr. Koelling, former student Panayiotis Kolliopoulis, and his graduate student, Varun Venoor, have provided me throughout the course of this project. The experiments could not have been completed without the help from the department's design engineer, Leigh Evard, who took the time to assist me. I would also like to thank my peers David Ellison, Steven Shi and Eugenia Stanisauskis for their gracious assistance throughout. I also could not have done this without my mom, dad and sister and their encouragement and support. Additionally, I would like to thank the friends I have made in CBE, especially Griffin Jenkins, that have become my second family and have helped me to become a better student and person.

Vita

2013 ..... Massillon Jackson High School

2017 ..... B.S. Chemical Engineering, Ohio State University

Fields of Study

Major Field: Chemical and Biomolecular Engineering

Table of Contents

List of Tables

List of Figures

Chapter 1: Introduction

Used as an alternative to conventional injection molding, gas-assisted injection molding (GAIM) is a process that injects pressurized gas into a mold cavity filled with molten polymer to create a hollowed core [1]. An image of the process is shown in Figure 1. Compared to conventional molding methods, GAIM maintains a reduction of material costs, yields a stronger product due to lower uniform residual stress distribution, and can reduce pressure usage by 75% [2]. It can be used to make durable automotive parts, instruments used in the medical field and consumer appliances in a wide array of geometries [3].

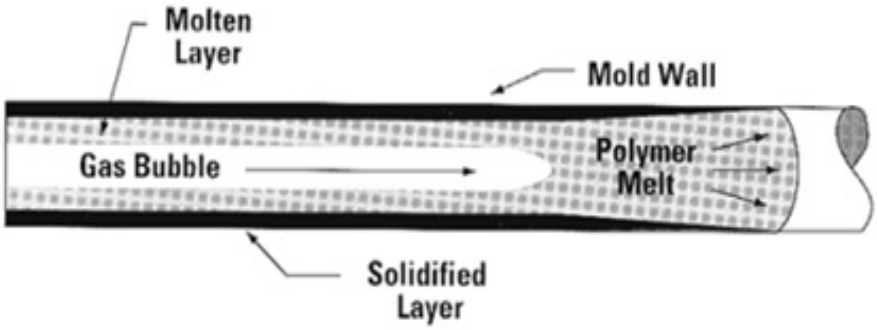

Figure 1: Depiction of gas-assisted injection molding process and parameters [11].

The industrial practicality of GAIM requires a reliable and repeatable process, but that can be difficult to attain because of its complexity and reliance on a multitude of variables and parameters [2]. Fractional coverage, m, is defined by Equation 1 below,

where R_b is the bubble radius and R_0 is the inner tube radius. It depends on the temperature gradient, delay time, polymer fluid type and the capillary number used.

$$m = 1 - \frac{R_b^2}{R_0^2} \quad (1)$$

Capillary number is the ratio of viscous forces to interfacial surface tension, σ, and is a strong function of the gas bubble speed, U_b, and fluid viscosity, μ.

$$Ca = \frac{U_b \mu}{\sigma} \quad (2)$$

Another important parameter for GAIM is Bond number, a dimensionless number characterizing the ratio of interfacial tension to gravitational forces. A Bond number greater than 1 indicates gravitational forces dominate the surface tension, and is undesirable. Using Equation 3 below where g is gravitational acceleration, R_0^2 is inner tube radius, ρ_L is the fluid density, and σ is interfacial tension, Bond number was calculated for each tube with the surface tension of each fluid used.

$$Bo = \frac{\rho_L g R_0^2}{\sigma} \quad (3)$$

To resolve the complexity of GAIM, simulation software was developed to predict fractional coverage with desired initial conditions. The downfall of models, such as MOLDFLOW and MOLD3DX, is their inability to calculate the correct fractional coverage in a non-isothermal system [4]. Real world GAIM is, however, a non-

isothermal process when a hot polymer enters a cooler cavity [6]. An accurate simulation can eliminate the need for current trial and error processes, saving time and resources. The research done by Panayiotis Kolliopoulos addressed these issues by developing a MATLAB simulation that determines fractional coverage in non-isothermal conditions for Newtonian and power law fluids. [5]. It has accurately predicted the fractional coverage of non-isothermal, Newtonian data obtained by Minesh Tendulkar at high capillary numbers [6].

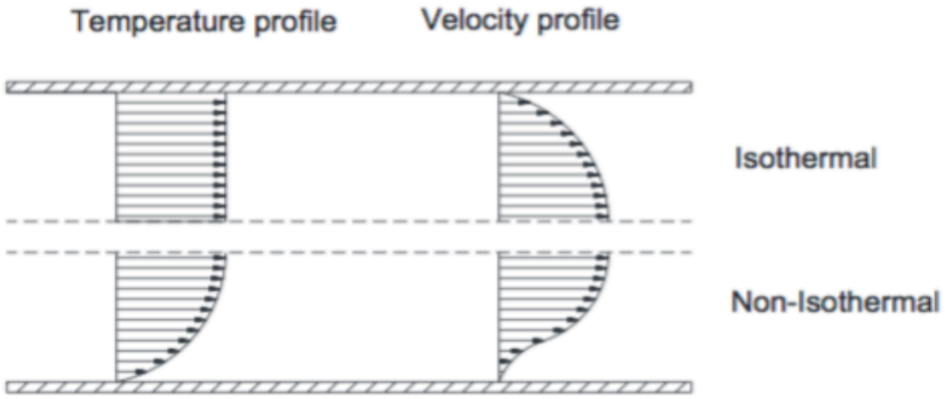

Figure 2: Isothermal and non-isothermal velocity and temperature profiles [5].

Although the simulation was modified for non-Newtonian fluids at high capillary numbers and non-isothermal systems, there was no existent experimental data to back up its accuracy and to check if the modifications can be applied to low capillary numbers. This research analyzes the experimentation of Newtonian, non-isothermal systems at low capillary numbers. The integration of these experiments with the simulation model will further progress the GAIM process towards more realistic and practical applications.

Chapter 2: Literature Review

The first to experiment gas penetration of Newtonian fluids were Fairbrothers and Stubbs in 1935 in isothermal conditions [12]. Their research determined the empirical relation of $m = 1.0(Ca)^{1/2}$ between the fractional coverage and viscous/interfacial tension forces. The fractional coverage was defined as ratio between the coated cross section to the total cross-sectional area.

Next, in 1960, Taylor explored the effects of different viscosity fluids in different diameter tubes [13]. He determined the previous correlation by Fairbrothers and Stubbs was only sufficient at low capillary numbers and not high. At high capillary numbers, he observed an asymptotic fractional coverage value of 60% as shown in Figure 3 below.

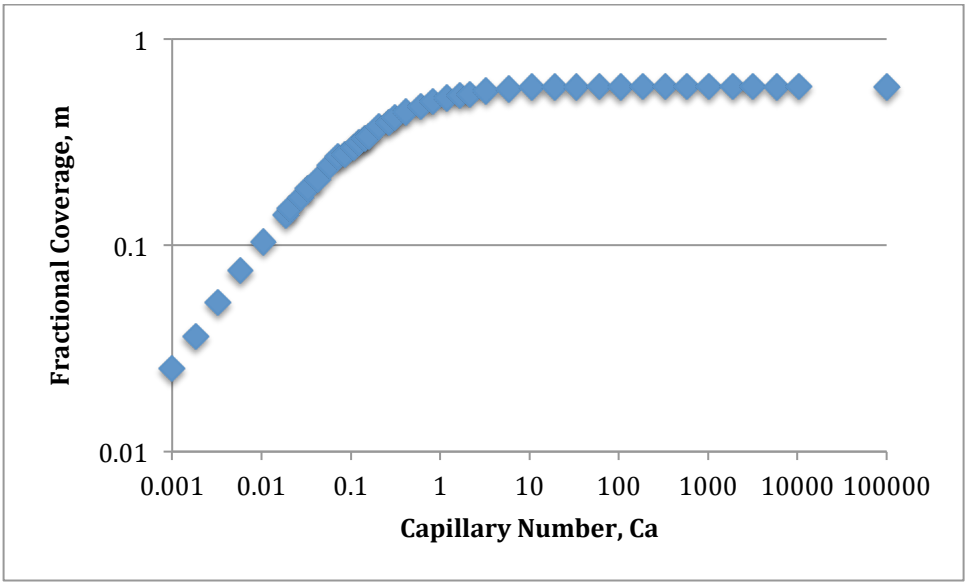

Figure 3: Asymptotic relationship for capillary number vs. fractional coverage by Taylor [13]

Next, Bretherton analyzed the GAIM process at low capillary numbers in 1961 [14]. To neglect the effects of gravity, the experiments were performed in small diameter vertical tubes or wider vertical tubes. The results of his experiment were a better established a theoretical relationship for bubble velocity at low capillary numbers, but were not accurate for high capillary numbers.

In 1995, Poslinski and Coyle conducted numerical simulations of GAIM in isothermal conditions [7]. They were able to generalize a Newtonian fluid model between capillary numbers 0 to 10^3. They used the Newtonian results as a basis of comparison for power-law fluids. Then, Huzyak and Koelling studied shear thinning and elastic effects in isothermal GAIM [8]. Their flow visualization studies helped to establish the elasticity and shear-thinning effects on flow patterns at various capillary numbers.

The experimental data of Minesh Tendulkar was later used by Yijie Wang to study and develop a model for Newtonian fluids that exhibited non-Newtonian properties when introduced to a temperature gradient at high capillary numbers [9]. As shown in Figure 2, there are distinct differences in fractional coverage between isothermal and non-isothermal systems at high and low capillary numbers. A significant amount of experimentation and simulation has been done for GAIM, but experiments of non-isothermal conditions at low capillary numbers is absent.

Chapter 3: Experimental Materials and Methodology

3.1 Experimental Apparatus

The apparatus used to study the non-isothermal gas bubble of Newtonian fluids at low capillary numbers is shown Figure 3 below. It contains two water baths; one of room temperature and one heated by a Fisher Scientific ISOTEMP 2100 temperature controller with built in circulator. The room temperature bath is where the observed gas bubble penetration occurs. It is a modification of what was used by Minesh Tendulkar (1997) during his study of non-isothermal GAIM at high capillary numbers.

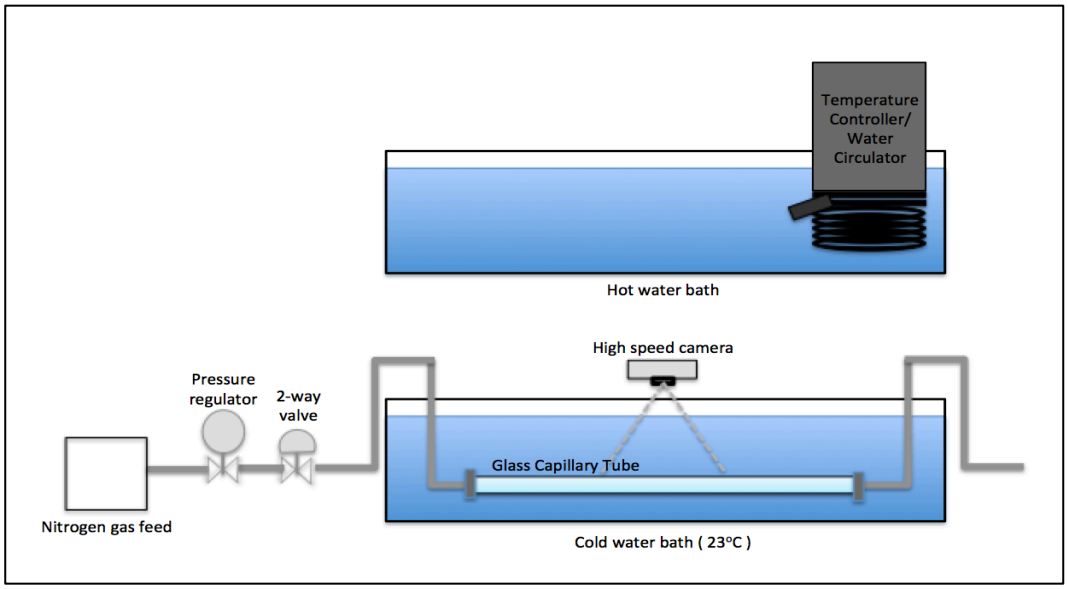

Figure 4: Experimental apparatus for low capillary experiments

Similar to prior apparatuses, the experiments were conducted in a tube with a capillary geometry. Because the gas injection was at low capillary numbers, the same assumption of asymptotic fractional coverage at high capillary numbers could not be

made. While previous experiments had used stainless steel capillary tubes, glass tubes were chosen to easier observe the behavior of the GAIM process at non-isothermal, low capillary numbers. The bore glass tubes of three different diameters were used, but all tubes had a length of 30.50 cm and can be seen in Figure 5 below. The outer diameters varied from 0.70 cm, 1.0 cm, and 1.3 cm and the respective inner diameters were 0.50 cm, 0.80 cm and 1.1 cm.

Figure 5: Experimental glass tubes from largest to smallest

Each tube edge was fitted with hose sized to its outer diameter, and it was connected to a barbed tube-to-male thread 90^{o} elbow adaptor as shown in Figure 6. This made removable connections between the outlet and gas inlet for each of the tubes. This let the tubes be easily removed to inject polymer into and cleaned between each trial. Fix

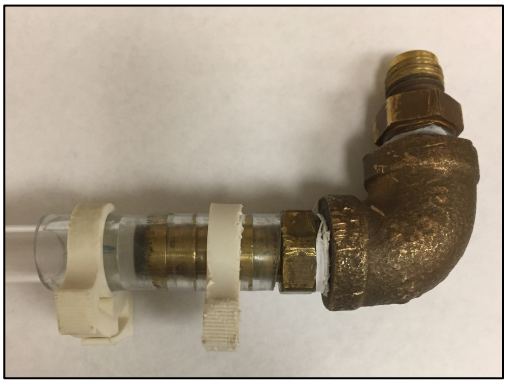

Figure 6: The connection used to connect the glass tubes to its gas inlet and outlets

The inlet end of each elbow adaptor was connected to a valve and a pressure regulator via Swagelok fittings. A hose linked the regulator to in-house Nitrogen gas coming in at 100 psi. A restriction tube was attached to the glass tube outlet, and was used to prevent the bubble velocity from reaching an infinite velocity. The length and diameter of the restriction tube were chosen such that the volumetric flow rate ratio between the tube inlet and outlet (Q_F/Q_I) was a value less than 1.1 in Equation 4. A ratio of 1.1 indicates the final flow rate will vary by less than 10% of the initial flow rate in the tube.

$$\frac{Q_F}{Q_I} = \left(\frac{L_1}{R_1^4} + \frac{L_2}{R_2^4}\right)/\left(\frac{L_2}{R_2^4}\right) \qquad 4$$

The volumetric flow rate in the tube including the restriction tube is represented by Q_I, and the flow rate in only the restriction tube is Q_F. The lengths of the glass tube and restriction tube are indicated by L_1 and L_2, and their respective radii are R_1 and R_2. Shown in Table 1, the length of the restriction tube with each of the varying glass tubes.

Table 1: Calculated ratio of initial flow rate to final flow rate of each glass tube

Tube Diameter (mm)	$\boldsymbol{Q_F/Q_I}$ **ratio**
5	1.0347
8	1.0051
11	1.0017

To determine the initial gas pressure required for the desired capillary number, Equation 5 below was used to solve for the pressure drop, ΔP, between the tube entrance and the restriction tube outlet. The tube cross-sectional area and calculated bubble velocity obtained from a specified capillary number were used to determine the initial tube volumetric flow rate.

$$Q_I = \frac{\pi \Delta P}{8\mu\left(\frac{L_1}{R_1^4} + \frac{L_2}{R_2^4}\right)} \qquad 5$$

3.2 Experimental Procedure

For every trial, the desired fluid was injected into the threaded end of the elbow adaptor connected to the tube by a syringe. The glass tube was angled during fluid injection to ensure no air bubbles were present. When the tube was filled, the elbow adaptor threaded ends were connected.

An important parameter in every trial is Fourier number, a dimensionless number characterizing the transient heat conduction. The fluid-filled tube was determined to be

uniform in temperature when it reached a Fourier number of 1. Fourier number, Fo is shown by Equation 6 below. In the below Equation, α is thermal diffusivity of the fluid, θ is time after placement in the water bath, and R_0 is the tube radius. The glass tube wall thickness was also factored into the calculation and was accounted for during experimentation.

$$Fo = \frac{\alpha\theta}{R_0^2} \qquad 6$$

To observe and characterize the gas-assisted injection process, a Google Pixel high-speed camera (1080 p, 240 fps) was placed 7 inches above the apparatus. To obtain better contrast of the fluid against the tube wall, water-soluble green coloring was added to the fluids. Every glass tube was fitted with two pieces of tape that were set a known distance from each other. This distance would be used to determine the bubble velocity by the amount of time it would take the bubble to traverse the known distance.

The gas pressure entering the tube controlled the speed of the gas bubble in the tube. Pressure was varied to obtain a desired capillary number for each of the tubes. The pressure regulator controlled the injection gas pressure, and pressure ranged from 1.25 to 15 psi. Maximum pressure was limited to 15 psi, because the glass tubes had pressure limitations that could not be exceeded. As a result, very high capillary numbers could not be obtained from the apparatus. In the event that the tubes shattered, safety precautions were taken during experimentation. Along with partially covering the water bath with a lid, safety glasses and proper PPE was worn.

3.2.1 Isothermal Trials

Because extensive research has been conducted on GAIM in isothermal conditions, the isothermal trials were used as a check and calibration of the apparatus. For every tube diameter and fluid, three trials with capillary numbers ranging from 0.01 to 1 were performed. The known theoretical and experimental relationship between fractional coverage and capillary number of Newtonian fluids is shown in Figure 3. This known relationship will be used as a visual calibration of fractional coverage for the non-isothermal experiments.

3.2.2 Non-Isothermal Trials

To create a temperature gradient, the tube was initially placed in the first hot water bath. The tube remained in the water bath for an amount of time long enough to obtain a Fourier number of 1. Once it was reached, the tube was quickly transferred to the second, room temperature water bath (23°). The temperature gradient of the two water baths ranged from 75 to 23°C and 50 to 23°C.

The delay time the tube rested in the second water bath before gas was injected was dependent on the desired Fourier number of that specific trial. For each fluid, the Fourier number varied from 0.01 to 1.0, which corresponded to the delay time ranges shown in Table 2 below.

Table 2: Corresponding delay time range for Fourier range 0.01 to 1

Fluid	**Fourier Range**	**Delay Time Range (s)**
65% Corn Syrup/Water	0.01 to 1.0	0.543 – 53.49
50% Glycerol/Water	0.01 to 1.0	0.589 – 58.93

Chapter 4: Fluid Characterization

Due to the pressure limitation of the glass tube, the fluid in the tube could not have a high viscosity. To satisfy these requirements, the chosen fluids were an aqueous glycerol (Fisher Scientific, G33-500) and an aqueous corn syrup (Kroger light corn syrup) solution. An Anton-Par MCR-300 rheometer was used to measure the dynamic viscosity of the fluids at varying temperatures. A steady shear regime ranging from 10^2 sec^{-1} to 10^3 sec^{-1} measured the viscosity using a temperature controlled 25 mm couette.

The viscosity of each fluid was measured at the varying temperatures of 23°C, 35°C, 50°C and 75°C. For a temperature of 23°C, the zero-shear viscosity of the glycerol solution is .0055 Pa*s and the corn syrup solution is .0232 Pa*s. The plot of shear behavior is shown in Figure 7 for the glycerol solution and in Figure 8 for the corn syrup solution.

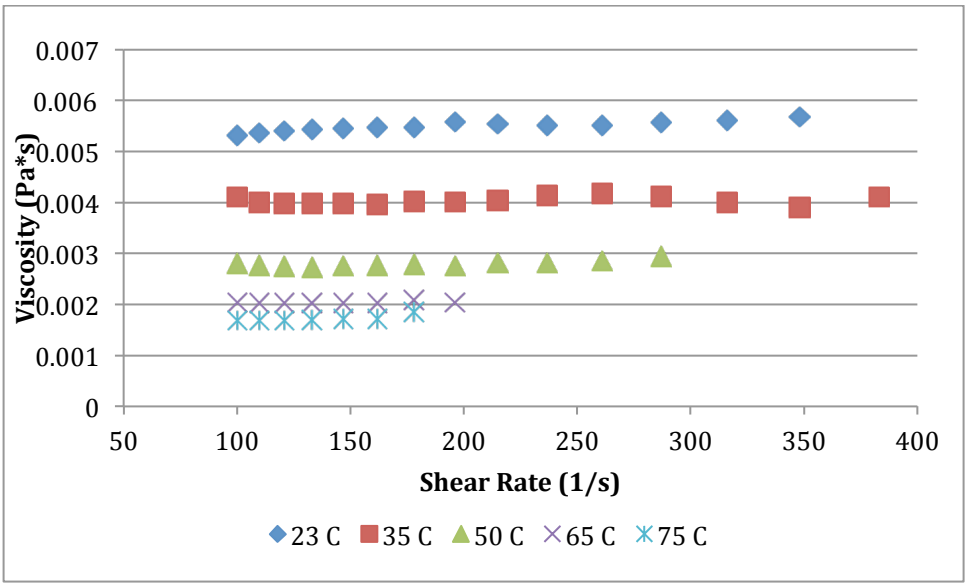

Figure 7: 50% Glycerol steady shear rate vs. viscosity for vary temperatures

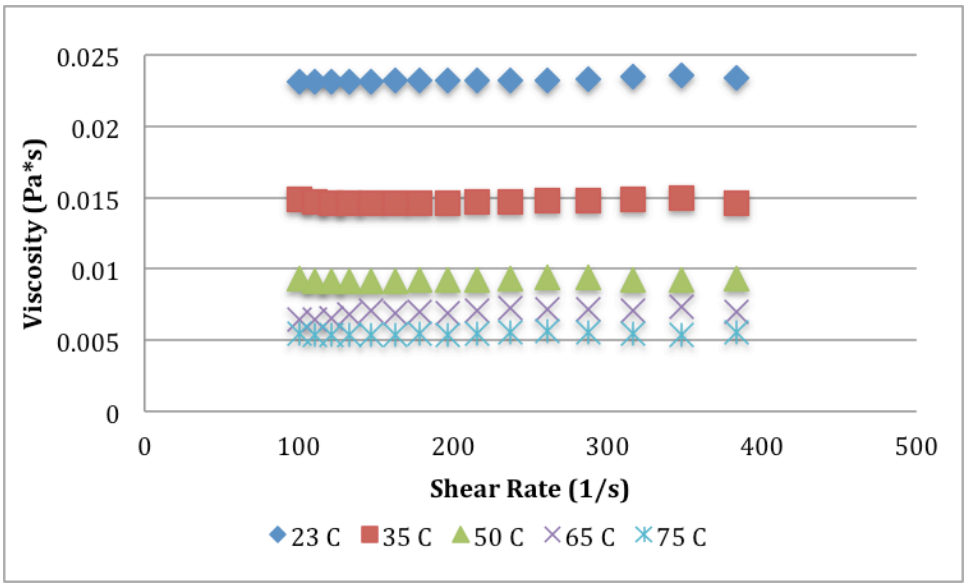

Figure 8: 65% Corn syrup steady shear rate vs. viscosity for vary temperatures

Both solutions maintained a constant velocity as the shear rate increased and an increase in viscosity as the temperature decreased. The trend observed reflects Newtonian shear dependence for the fluids that will allow for an assumption of asymptotic fractional coverage of 0.6 in isothermal conditions.

4.1 Fluid Temperature Dependence

The relationship between viscosity and temperature for corn syrup and glycerol is plotted in Figure 9 below. It represents the inverse temperature as a function of logarithmic viscosity.

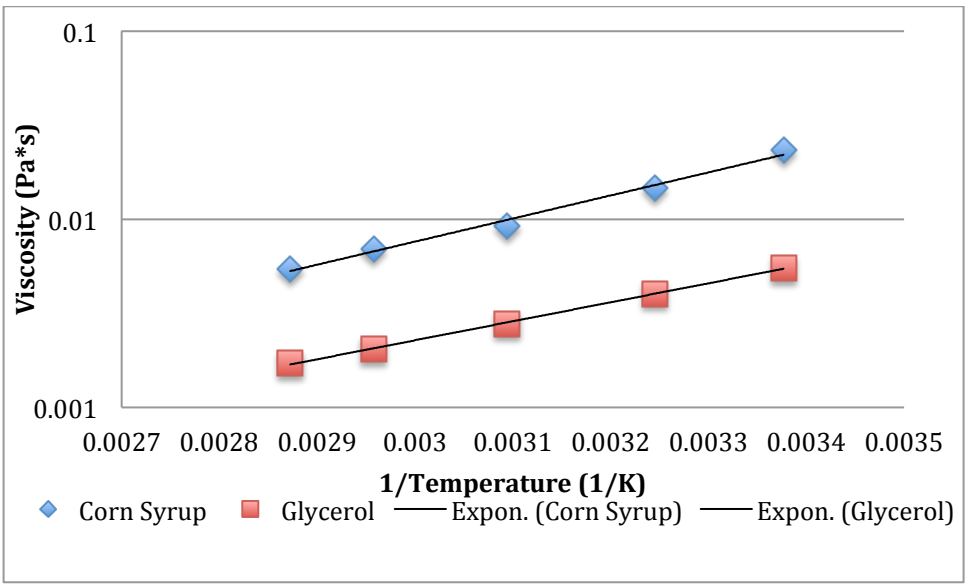

Figure 9: Viscosity vs. inverse temperature fitted with Arhennius model

The temperature dependence of viscosity can be fitted with the Arrhenius model in Equation 7 below. From the model, viscosity at varying temperatures can be determined. The pre-exponential factor, A, is the frequency factor and the flow activation energy is represented by $\Delta H/R$. Increasing the flow activation energy increases the temperature sensitivity, and the two fluids have slight differences in their sensitivity. The glycerol solution has a flow activation energy of 2324 K, while the corn syrup solution has a flow activation energy of 2824 K. Gas penetration of fluids with differing rheological properties broadens the scope of experimentation.

$$\eta(T) = Ae^{\left[\frac{\Delta H}{RT}\right]} \quad 7$$

Surface tension of the two fluids was obtained from literature of the aqueous solutions. At 25°C, the glycerol has a surface tension of 67.4 mN/m and the corn syrup

has a surface tension of 72.0 nN/m. The density for each fluid was determined by taking the mass of a known volume of each fluid. An overview of each fluid's properties is in Table 3 below.

Table 3: Fluid properties at 25°C for glycerol and corn syrup solutions

Properties	**50% Glycerol**	**65% Corn Syrup**
Viscosity at 25°C (mPa*s)	5.50	23.2
Density at 25°C ($\frac{kg}{m^3}$)	1125.5	1211.3
Thermal conductivity at 25°C ($\frac{W}{mK}$)	0.450	0.540
Specific heat at 25°C ($\frac{J}{kgK}$)	3800	3000
Surface Tension at 25°C ($\frac{mN}{m}$)	67.4	72.0
Frequency Factor $(Pa * s)$	2.13E-6	1.59E-6
Flow Activation Energy (K)	2324.0	2824.0

Chapter 5: Results and Discussion

5.1 Analysis of the Gas Bubble

The high-speed videos of the process analyzed two important parameters: the gas bubble velocity and the wall thickness. Bubble velocity was determined by the amount of time it took the bubble tip to traverse a known distance in the tube. With the bubble velocity, surface tension and fluid viscosity known, the capillary number could be calculated.

Because the experiments were conducted in glass tubes, wall coverage was determined by capturing video of the process and analyzing the image captured. An image of a trial is shown below in Figure 10. The process of measuring the wall thickness involved setting the known outer tube diameter as scale. The dark shadow following the gas bubble would be measured to determine the coating thickness. Each fluid, however, refracted light differently. To accurately measure the fractional coverage, calibrations were made for each fluid from known data gathered from previous isothermal trials.

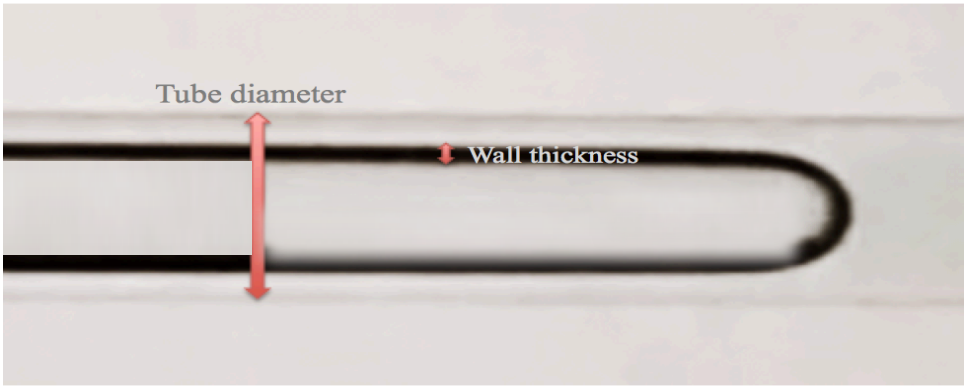

Figure 10: An image used to determine wall thickness from a glycerol trial

5.2 Isothermal experiments

The purpose of the isothermal experiments is to observe the fluid behavior at different process conditions and to establish a calibration for the fractional coverage.

5.2.1. Bond number

Bond number was calculated for each tube using the surface tension of each fluid used. Both the 8 mm and 11 mm diameter tubes had Bond numbers exceeding a value of 1 for both the glycerol and corn syrup solutions. The experiments using these tubes reflected a large Bond number, because pooling of fluid at the bottom layer of the tubes was observed as shown in Figure 11. The experimental results matched what was expected from the theoretical Bond numbers. It was determined that these two larger diameter tubes would yield inconclusive and inaccurate results if continued for experimentation. As a result, only the smaller diameter tube was used for further analysis.

Figure 11: Side view of wall coating on glass tube after gas injection with Bo <1 and with Bo>1

5.2.2. Wall thickness calibration

Earlier experiments by Taylor and Cox and Poslinski established the theoretical and experimental relationship between capillary number and fractional coverage in isothermal systems, shown in Figure 12 below. For any Newtonian fluid, the fractional coverage can be determined as long as the capillary number is known for that trial.

As shown in Figure 12, the capillary number for every trial was plotted against the already known correlation to determine what the fractional coverage should be. This value was used with the measured thickness from the video to establish a relationship between what is visually measured and what the actual is. The need for this calibration is due to the refraction of light from each of the fluids in the tube and the water in the bath, so the visually measured thickness is not the true thickness. This calibration was further used to determine wall thickness during non-isothermal trials.

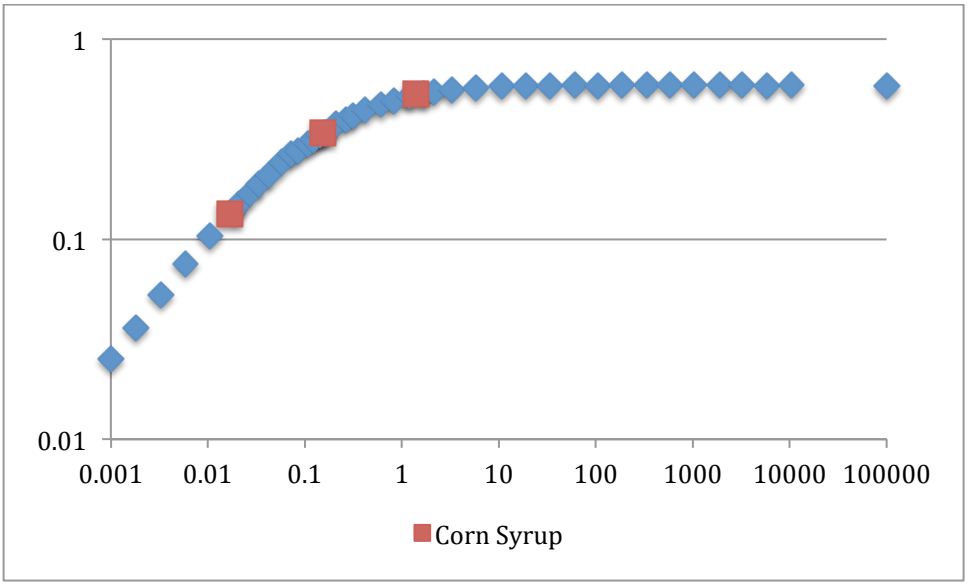

Figure 12: The method of obtaining fractional coverage from a known Ca for corn syrup

5.2.3 Experimental observations

Although the larger tubes experienced a larger than desirable Bond number, multiple trends were observed. Keeping the gas injection pressure constant, the bubble speed increased greatly as the glass tube diameter decreased. This can be attributed to the greater volume of fluid being restricted by the restriction tube for the larger tubes. As the speed increased, the capillary number also increased and the resulting fractional coverage increased as well.

For a constant tube diameter, increasing gas injection pressure will increase the velocity of the penetrating bubble. Shown in Figure 13, the measured wall thickness was found to increase in size as the bubble velocity increased, reflecting trends from previous experiments. The solution with a higher viscosity had a slower bubble velocity than the less viscous fluid. The higher viscosity fluid provides a greater resistance against the bubble, so it moves through the fluid at a slower pace.

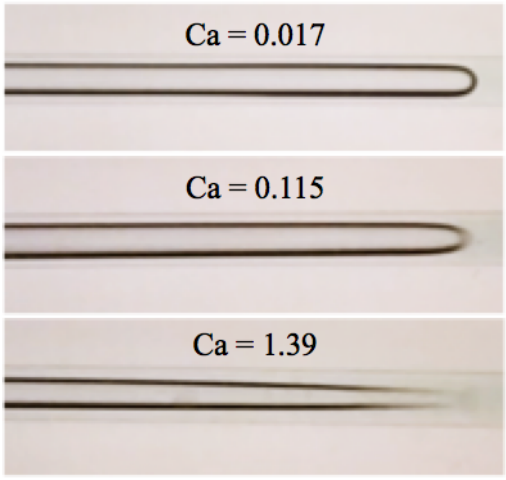

Figure 13: Corn syrup at varying Capillary numbers (0.02, 0.11, 1.39)

5.3 Non-Isothermal Experiments

Many parameters were observed and calculated from the results of the non-isothermal experiments. Images taken from the non-isothermal experiments are shown in Appendix A. They exhibit a slight change in the shape of the bubble front compared to the isothermal velocity profiles, as a frozen layer forms due to the temperature gradient in the tube.

5.3.2 Effect of Fourier Number and Delay Time

The delay time influenced the fractional coverage for every non-isothermal trial conducted. Fourier number is dependent on delay time, so a range of $0 < Fo < 1$ corresponds to a delay time range of $0 < t < 60$. In Figure 14 and Figure 15 for corn syrup, it is observed that every trial exhibited a maximum fractional coverage and began to decrease until it reached the asymptotic value associated with its capillary number.

Noticeable trends of the delay time are that a maximum fractional coverage occurs for almost every trial at approximately 6 seconds ($Fo \sim 0.10$). Previous studies by Minesh Tendulkar at high capillary numbers indicated a maximum fractional coverage at a Fourier number of 0.08. An explanation for this phenomenon is the formation of a frozen layer due to the temperature differences of the two baths when the outside of the tube is cold and the center fluid is still hot. Another trend observed is the leveling off of the fractional coverage at a Fourier number of 1. Fourier numbers of 0 and 1 are considered isothermal, because the entire apparatus becomes the temperature of its

surrounding water bath. However, a Fourier number of 0 equates to a delay time of 0 seconds, and is not experimentally achievable.

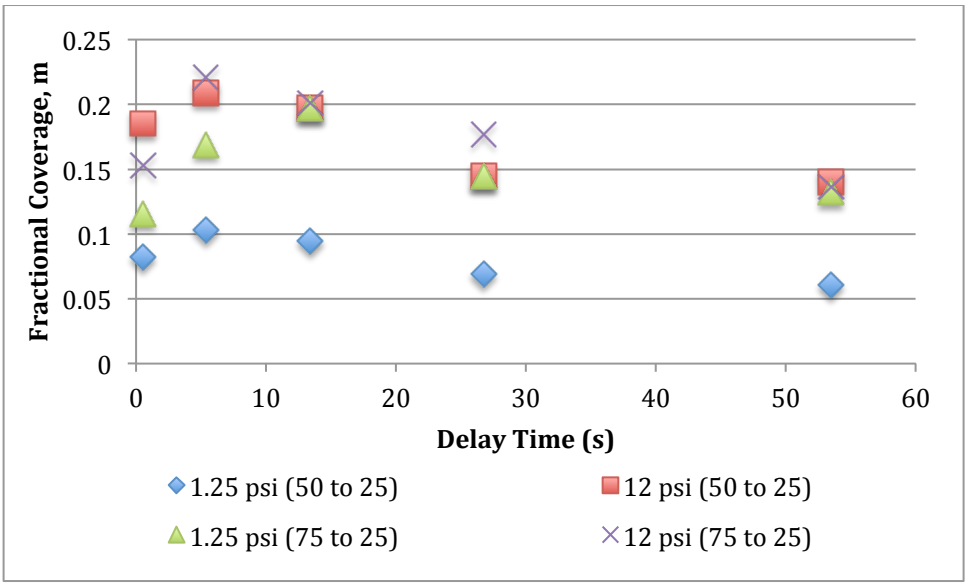

Figure 14: Corn Syrup solution fractional coverage vs. delay times at different Ca and temperatures

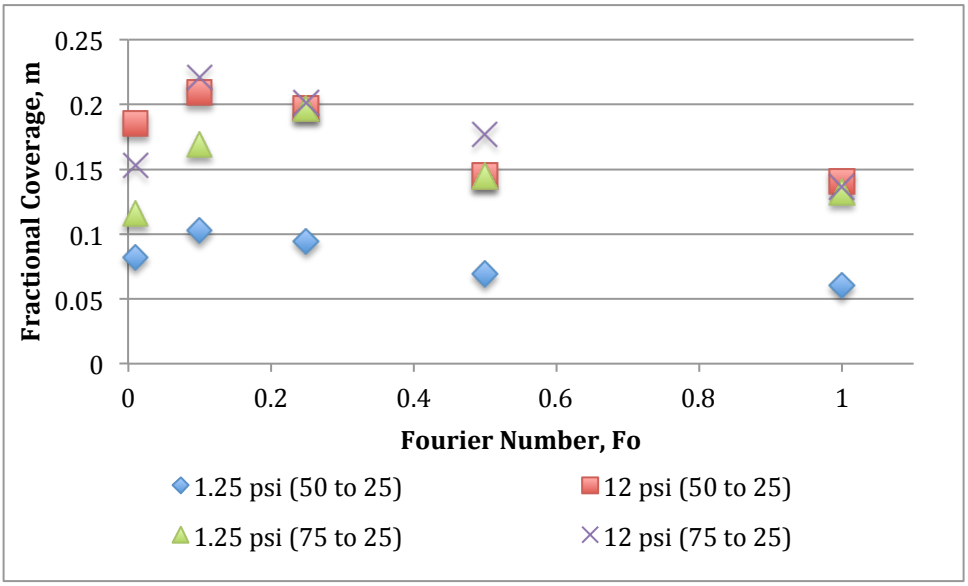

Figure 15: Corn Syrup solution fractional coverage vs. Fo number at different Ca and temperatures

For consistency in the calculation of capillary number, the viscosity at 23°C was used. There will be error in this method, because the viscosity is changing and not uniform in the tube. As a result, every trial in Figure 14 and Figure 15 did not have the same capillary number for a given gas injection pressure due to changing viscosity for different delay times.

5.3.2 Effect of Temperature Gradient

The effects of the temperature gradient can be observed from the previous figures. For both glycerol and corn syrup, there is a larger fractional coverage when the gradient is 75 to 25°C than when it is 50 to 25°C. Similar trends were observed in Minesh's experiments as well, when the maximum fractional coverage attained was with a gradient of 65 to 25°C. Increasing the gas injection pressure also had an effect on the fractional coverage, and can be explained by the increased capillary number.

5.4 Model

The model utilizes a hybrid control-volume finite element/finite-difference method, a momentum balance and applies heat transfer governing equations. It assumes an asymptotic fractional coverage of 0.6 when capillary number is greater than 10. It also implements a frozen layer model in non-isothermal system to account for the fractional coverage change with different delay times. In this model, deviation from the parabolic

shape of the velocity profile is due to the change of temperature continuously in the radial direction [5].

To determine the frozen layer thickness, the finite difference method was used split into three heat transfer regions. The first region is accounts for heat transfer outside of the tube and the governing equation for it is in Equation 8 below. The thermal conductivity is k_g of the glass tube, outer tube radius is R_{out}, convective heat transfer coefficient of the layer just outside the tube is h, T_w is the tube wall temperature and bulk fluid temperature is T_B. Assuming the main heat transfer to be free convection to obtain h, the

$$-k_g \frac{\partial T_g}{\partial r}|_{r=R_{out}} = h(T_w - T_B) \quad (8)$$

The next region accounts for the heat transfer inside the glass tube and is represented by the governing Equation 9. The thermal diffusivity of glass is α_s, and T_s is the temperature of the glass tube.

$$\frac{\partial T_g}{\partial t} = \alpha_s \left(\frac{\partial^2 T_s}{\partial r^2} - \frac{1}{r} \frac{\partial T_s}{\partial r} \right) \quad (9)$$

Lastly, the third heat transfer region is inside the fluid and is represented by Equation 10 below. Fluid thermal diffusivity is α_f and T_f is the fluid temperature.

$$\frac{\partial T_f}{\partial t} = \alpha_f \left(\frac{\partial^2 T_f}{\partial r^2} - \frac{1}{r} \frac{\partial T_f}{\partial r} \right) \quad (10)$$

The temperature profile that corresponded to the bubble tip and edge was calculated by averaging the temperature profiles. The temperature effect on viscosity was then used to determine the velocity profile in the governing Equation 11. In this, ΔP is the pressure gradient and L is the tube length.

$$\frac{\partial}{\partial r}\left(r\eta\frac{\partial u_z}{\partial r}\right)=\frac{\Delta P r}{L} \tag{11}$$

The velocity profile is normalized by the Equation 12, where the normalized velocity is u^* and the new radius related to coating thickness is R_x.

$$u^*=1-\left(\frac{r}{R_x}\right)^2 \tag{12}$$

With the normalized velocity calculated, the equivalent volumetric flow rate is used in Equation 13 to find the new radius, R_x.

$$2\pi\int_0^{R_{in}} r u_z^* d=2\pi\int_0^{R_x} r u^*\,dr \tag{13}$$

With the new radius determined, the hydrodynamic fractional coverage is calculated using Equation 14.

$$m = 1 - \left(\frac{\sqrt{1 - m_\infty} R_x}{R_{in}}\right)^2 \quad (14)$$

5.4.1 Model vs. Experimental Results

The results of the experiment were input into the simulation, along with the fluid characteristics. It required a specification of the temperature and pressure gradient, and the asymptotic coverage of the fluid when the Fourier number was greater than 1 for a given capillary number. Running the simulations after entering the conditions gave the outputs shown in the following Figure 16 and Figure 17. The experimental data is plotted against the model prediction.

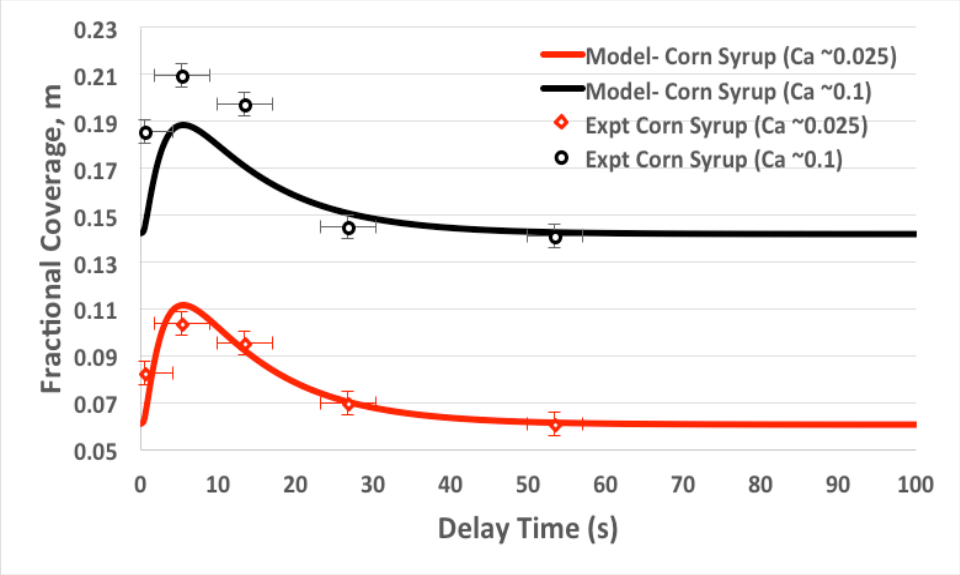

Figure 16: Corn syrup non-isothermal (50 to 25°C) delay time vs. fractional coverage

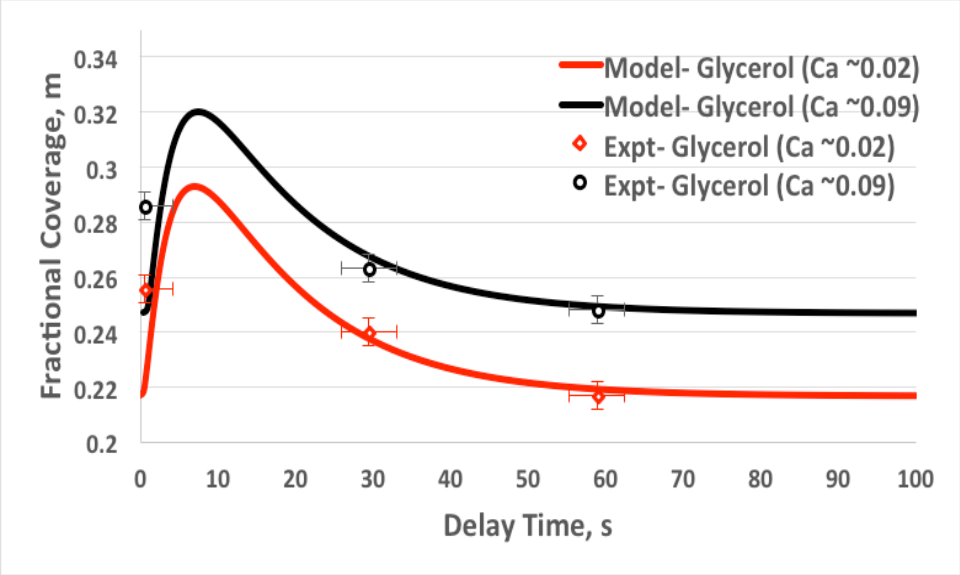

Figure 17: Glycerol non-isothermal (75 to 25°C) delay time vs. fractional coverage

When temperature was kept constant, the capillary number had an effect on the fractional coverage. The higher the capillary number, the greater the fractional coverage observed. This can be explained by the increase of bubble velocity due to the increase in pressure. As bubble velocity increased, the capillary number increased and caused the fractional coverage to increase. The remaining figures for corn syrup and glycerol are in the Appendix B and exhibit similar trends.

5.4.2 Model vs. Experimental Effects of Temperature Gradient

The relationship between the temperature gradient and the fractional coverage was examined with the capillary number kept constant. The effects of fractional coverage of a constant low capillary number for corn syrup and high capillary number for glycerol are shown in Figure 18 and Figure 19.

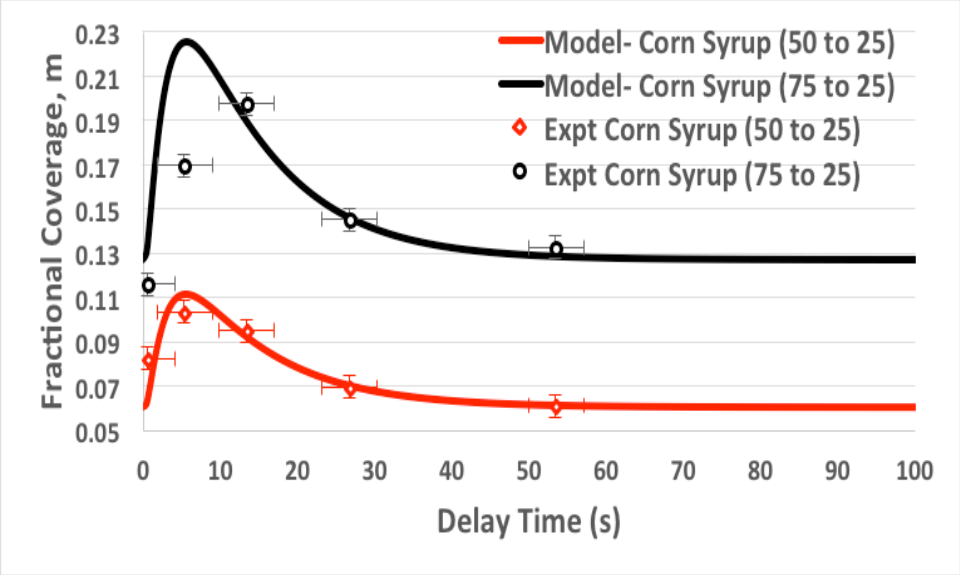

Figure 18: Corn syrup low capillary delay time vs. fractional coverage

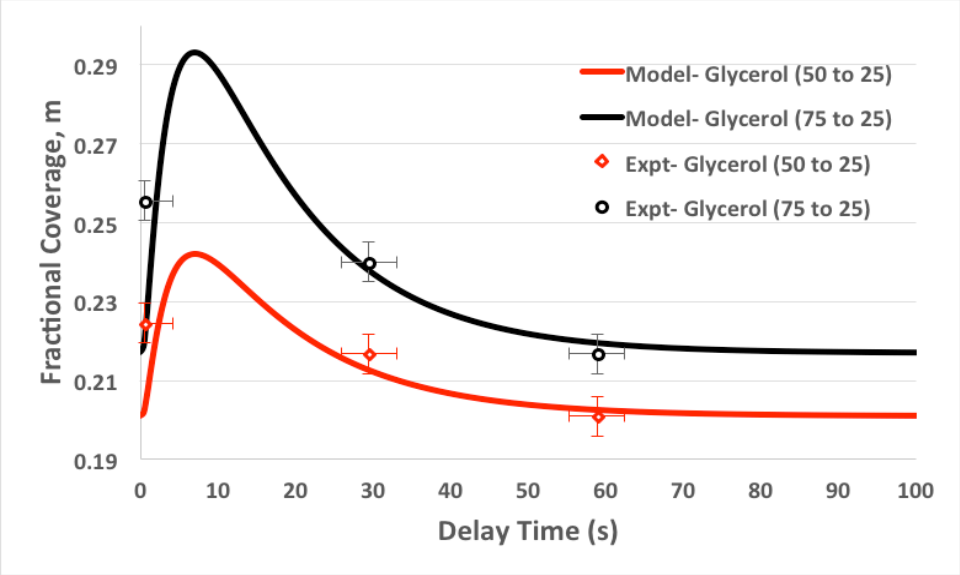

Figure 19: Glycerol high capillary delay time vs. fractional coverage

The larger temperature gradient increases the fractional coverage when the fluid is subjected to a similar capillary number. It is suspected that the temperature difference caused a larger frozen layer. The increase of fractional coverage can also be explained by

the lower viscosity caused by the higher temperature that provides less resistance the bubble so it travels through the tube faster. Similar trends were observed for the other trials shown in Appendix B.

5.4.1 Model vs. Experimental Effects of Fluid Temperature Sensitivity

The relationship between the temperature sensitivity and the fractional coverage was examined between the two fluids when the capillary number and temperature gradient were kept constant. The effects of fractional coverage of a constant low capillary number and constant high capillary number for glycerol and corn syrup are shown in Figure 20 and Figure 21.

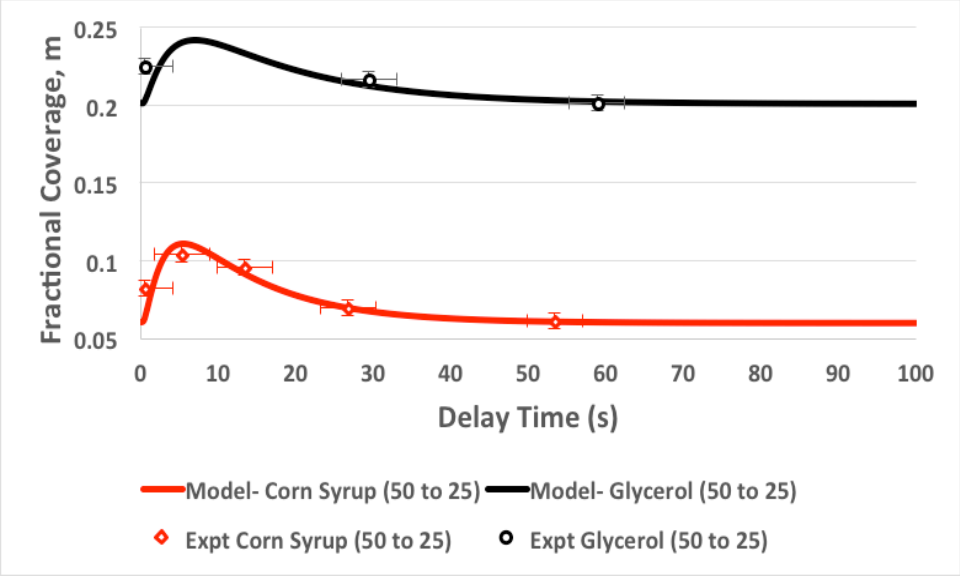

Figure 20: Low capillary (50 to 25) for corn syrup and glycerol

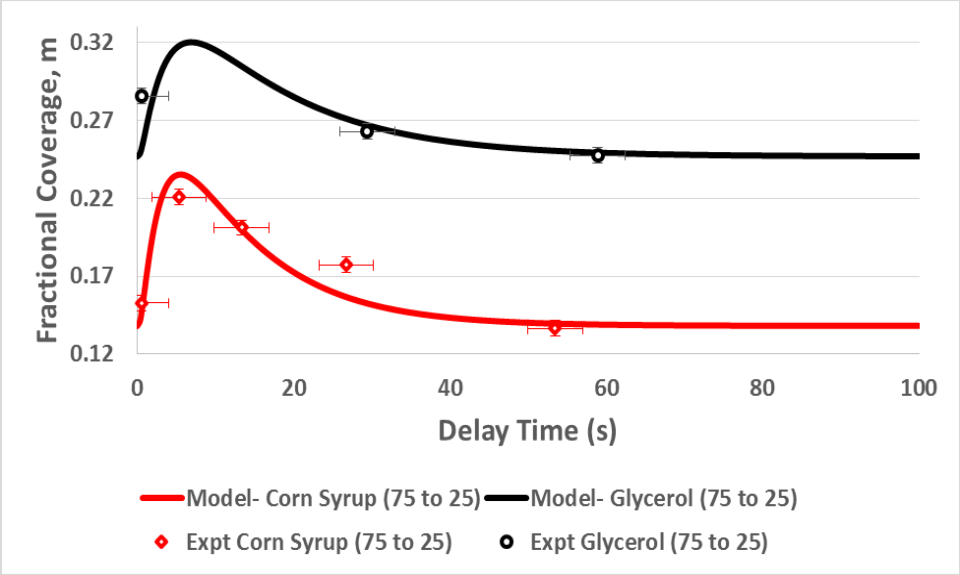

Figure 21: High capillary (75 to 25) for corn syrup and glycerol

When subjected to similar conditions of temperature and gas injection pressure, the glycerol has a higher overall coating thickness in comparison to corn syrup. This behavior can be attributed to the differences in viscosity of the two fluids. A lower viscosity fluid, such as the glycerol solution, provides a less resistance to the bubble than the corn syrup solution. Because the bubble has a greater speed, the capillary number increases and increases the overall fractional coverage. Similar trends are observed in the Appendix B when the capillary number and temperature gradient are fixed to examine the relationship between the two fluids.

The flow activation energy of the two fluids indicates a higher temperature sensitivity of the corn syrup compared to the glycerol solution. The results of the experiment confirm this as increasing the temperature gradient causes a greater increase in overall fractional coverage for corn syrup than it does for glycerol.

5.4.1 Overall Model vs. Experimental Results

The results of the simulation appear to follow the wall coverage obtained from experimentation decently. Although there are some deviations, they can be attributed to human error made during the experimental runs and from measuring the wall thickness by sight. The maximum deviation from the simulation to the experimental of fractional coverage is slightly below 15%. The simulation appears to be successful at predicting the general behavior of Newtonian fluids at high and low capillary numbers when compared to experimentation.

There are multiple sources of error in the experimental fractional coverage. Error bars have been placed on each experimental trial to account for the unavoidable error in the delay time and in the measuring of the fractional coverage.

Chapter 5: Conclusion and Future Work

5.1 Conclusion

The GAIM process was further explored by observing the behavior of a more realistic, non-isothermal system at high and low capillary numbers. The need for experimentation to determine the accuracy of the developed simulation was crucial. The model was successful in predicting fractional coverage for earlier, high capillary experiments. Now, with low capillary experiments, the simulation can generally predict the fractional coverage of a system with accuracy.

The trends observed during experimentation were similar to non-isothermal trials by Minesh Tendulkar. The delay time has a large effect on the fractional coverage of the process. The greatest fractional coverage occurred around a Fourier number of 0.1, where the maximum occurred at 0.08 in the high capillary number experiments.

For a constant temperature gradient, the effect of capillary number was observed. It was determined the fractional coverage exhibited a sharper increase when the capillary number was increased. For a constant capillary number, the larger temperature gradient played a larger effect on the maximum fractional coverage than the lower temperature gradient. When comparing the sensitivity of the two fluids, the corn syrup exhibited a higher overall fractional coverage increase when the temperature was increased.

For low capillary number experiments, the model appears to predict the process parameters well. With the high capillary experiments, it can be said to predict Newtonian fluids in non-isothermal systems accurately.

5.3 Future Work

Although non-isothermal systems are more realistic, the use of Newtonian fluids is limiting. The simulation model can also predict the behavior of non-Newtonian fluids as well, but there are no experiments to ensure its accuracy. Future experiments will be required in order to test its true capability. With the study of non-isothermal and non-Newtonian fluids established, future work can potential involve systems that are not at steady state.

There were some limitations to the current apparatus due to the use of glass tubes. High capillary number experiments could not be performed due to the low pressure that the glass could withstand. Future work should look into transparent tubes that can withstand higher pressures but can also easily observe the process for analysis. Further experiments in similar conditions as these will need to be tested for repeatability in results. This is will also work to reduce the error that is high prevalent throughout the process inherently.

References

[1] Loren, N. S. (1993). Patent No. US5204050 A. US.

[2] British Plastics Federation. “Injection Moulded (Gas Assisted).

[3] Hansen, M. (2005). “Gas-Assist Injection Molding: An Innovative Medical Technology.” *Medical Device & Diagnostic Industry.* Web.

[4] Jianhui Li, L. C. (2009). “Surface Model Based Modeling and Simulation of Filling Process in Gas-Assisted Injection Molding.” *Journal of Manufacturing Science and Engineering,* 1-8.

[5] Kolliopoulos, P. (2016). “Modeling and Simulation of Non-Isothermal Gas-Assisted Injection Molding for Non-Newtonian fluids.” The Ohio State University: BS. Thesis.

[6] Tendulkar, M. R. (1997). “Gas bubble penetration through Newtonian fluids under non isothermal conditions.” The Ohio State University: Doctoral Dissertation.

[7] Poslinski, AJ and Coyle, DJ. “Boundary conditions at gas-liquid interfaces in lubrication flows of non-Newtonian liquids.” GE Corporate Research and Development (1997), Schenectady, New York, 15-16.

[8] P.C. Huzyak, K. K. (1997). “The penetration of a long bubble through a viscoelastic fluid in a tube.” *Non-Newtonian Fluid Mechanics,* 73-88.

[9] Wang, Y. (2003). “The Effect of Non-Newtonian Rheology on Gas-Assisted Injection Modeling Process.” The Ohio State University: PhD. Thesis.

[10] Yamamoto, Takehiro, Takanori Suga, Kiyoji Nakamura, and Noriyasu Mori. "The Gas Penetration Through Viscoelastic Fluids With Shear-Thinning Viscosity in a Tube." *Journal of Fluids Engineering J. Fluids Eng.*126.2 (2004): 148. Web.

[11] "Gas Assist Injection Molding." Gas Assist Injection Molding. N.p., n.d. Web. Mar. 2017

[12] Fairbrother, Fred, and Alfred E. Stubbs. "119. Studies in electro-endosmosis. Part VI. The “bubble-tube” method of measurement." J. Chem. Soc. 0.0 (1935): 527-29. Web.

[13] Taylor, G. I. "Deposition of a viscous fluid on the wall of a tube." Journal of Fluid Mechanics 10.02 (1961): 161. Web.

[14] Bretherton, F. P. "The motion of long bubbles in tubes." Journal of Fluid Mechanics 10.02 (1961): 166. Web.

[15] Gauri, Vishal, and Kurt W. Koelling. "Gas-assisted displacement of viscoelastic fluids: flow dynamics at the bubble front." Journal of Non-Newtonian Fluid Mechanics 83.3 (1999): 183-203. Web.

Appendix A: GAIM Trials

Isothermal Trials

Glycerol

Figure 22: Glycerol isothermal trials at varying capillary numbers

Non-isothermal Trials

Corn syrup (50 to 25) Low Capillary

Figure 23: Corn syrup non-isothermal at low capillary (50 to 25°C)

Corn syrup (50 to 25) High Capillary

Figure 24: Corn syrup non-isothermal at high capillary (50 to 25°C)

Corn syrup (75 to 25) Low Capillary

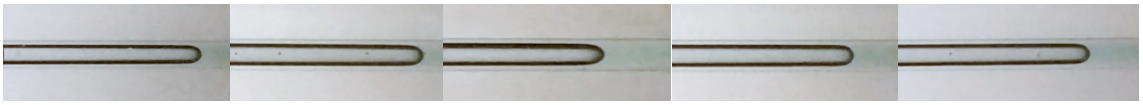

Figure 25: Corn syrup non-isothermal at low capillary (75 to 25°C)

Corn syrup (75 to 25) High Capillary

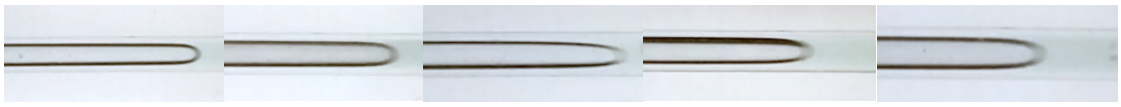

Figure 26: Corn syrup non-isothermal at high capillary (75 to 25°C)

Glycerol (50 to 25) Low Capillary

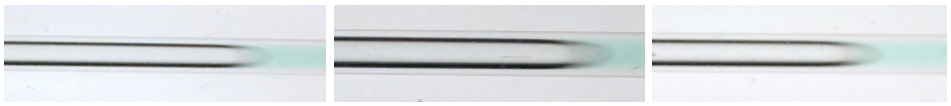

Figure 27: Glycerol non-isothermal at low capillary (50 to 25°C)

Glycerol (50 to 25) High Capillary

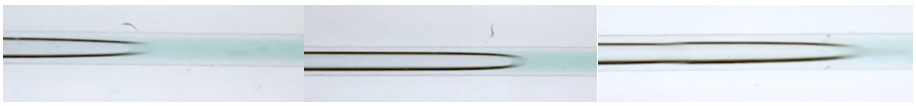

Figure 28: Glycerol non-isothermal at high capillary (50 to 25°C)

Glycerol (75 to 25) Low Capillary

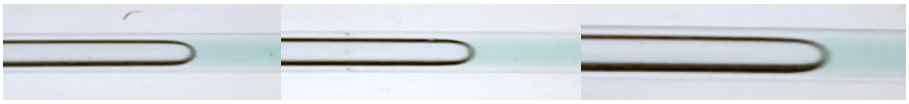

Figure 29: Glycerol non-isothermal at low capillary (75 to 25°C)

Glycerol (75 to 25) High Capillary

Figure 30: Glycerol non-isothermal at high capillary (75 to 25°C)

Appendix B: Model vs. Experimental Results

Constant Temperature Gradient, Different Capillary Number

A. Corn Syrup

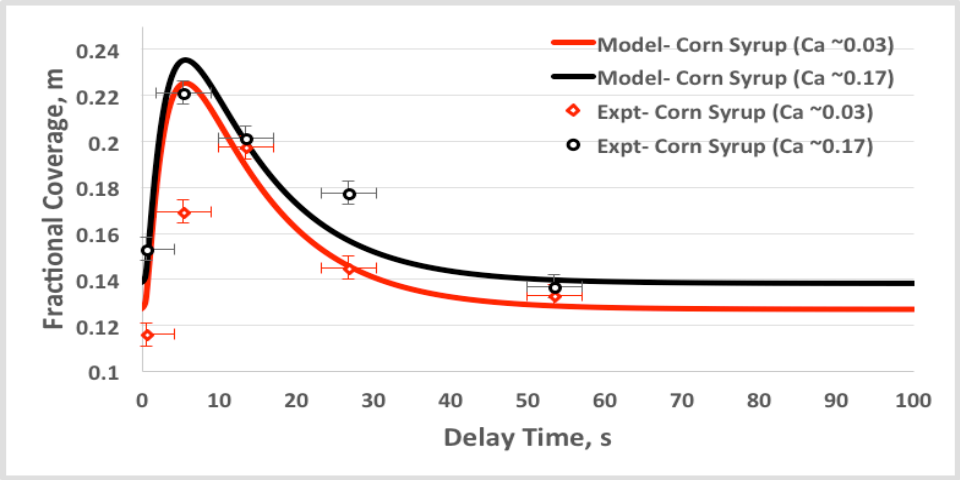

Figure 31: Corn syrup non-isothermal (75 to 25°C) delay time vs. fractional coverage

B. Glycerol

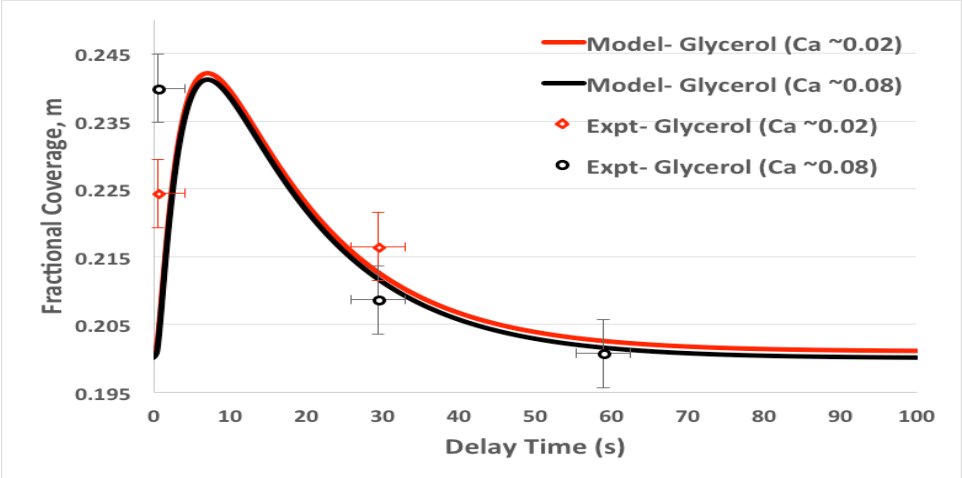

Figure 32: Glycerol non-isothermal (75 to 25°C) delay time vs. fractional coverage

Constant Capillary Number, Different Temperature Gradient

A. Corn Syrup

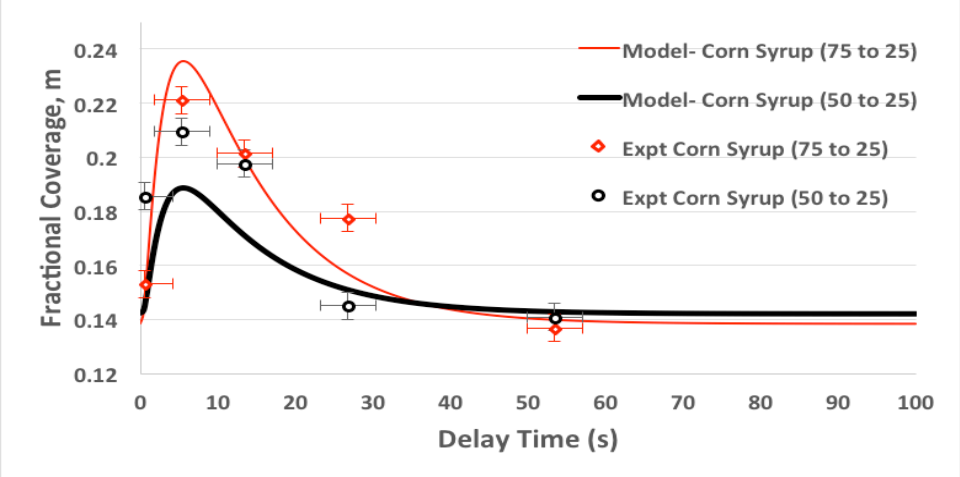

Figure 33: Corn syrup high capillary delay time vs. fractional coverage

B. Glycerol

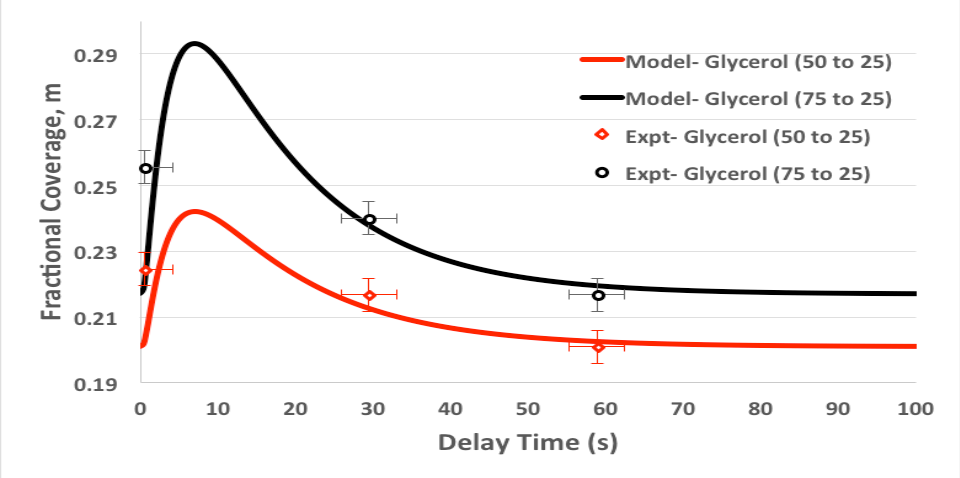

Figure 34: Glycerol lows capillary delay time vs. fractional coverage

Constant Capillary Number and Temperature Gradient, Different Fluid

A. Low Capillary

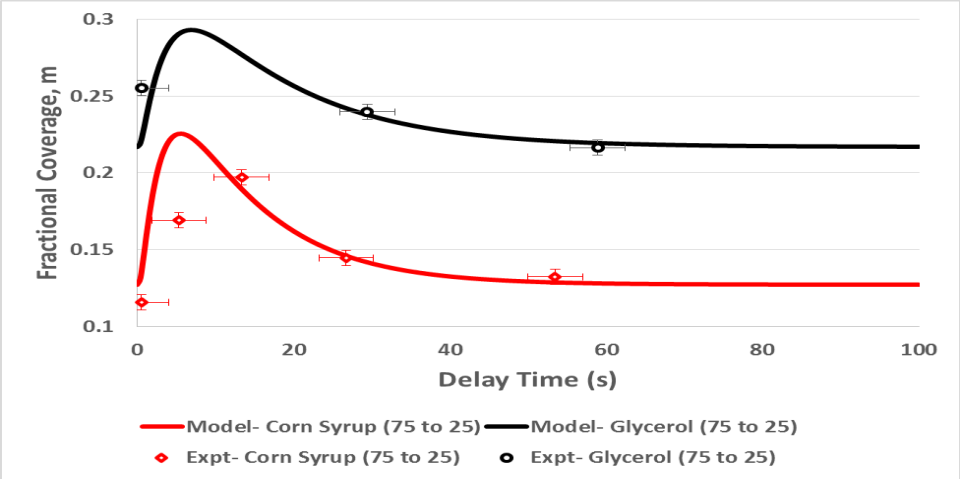

Figure 35: Low capillary (75 to 25) for corn syrup and glycerol

B. High Capillary

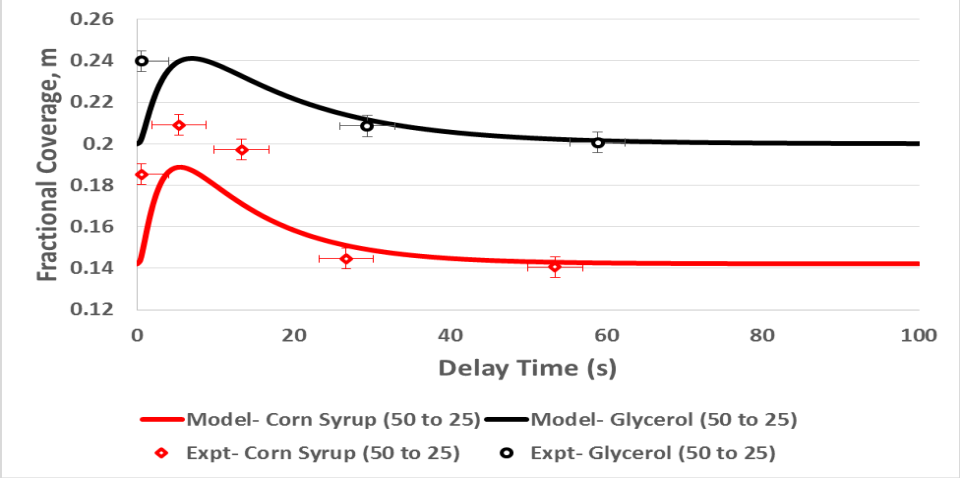

Figure 36: High capillary (50 to 25) for corn syrup and glycerol